

# Tropospheric Rossby Wave Breaking and Variability of the Latitude of the Eddy-Driven Jet

CHAIM I. GARFINKEL

*Department of Earth and Planetary Science, The Johns Hopkins University, Baltimore, Maryland, and Earth Science Institute, Hebrew University, Jerusalem, Israel*

DARRYN W. WAUGH

*Department of Earth and Planetary Science, The Johns Hopkins University, Baltimore, Maryland*

(Manuscript received 20 January 2014, in final form 17 June 2014)

## ABSTRACT

A dry general circulation model is used to investigate the connections between Rossby wave breaking and the latitude of the midlatitude tropospheric eddy-driven jet. An ensemble of experiments is constructed in which the jet latitude is influenced by a midlatitude tropospheric temperature anomaly that resembles observed climate change and by the imposition of a stratospheric polar vortex, and the distribution of Rossby wave breaking frequency is examined for each experiment. The shift in wave breaking per degree latitude of jet shift is then compared for three different sources of jet movement: the tropospheric baroclinic forcing imposed in midlatitudes, the imposition of a stratospheric polar vortex, and the internal variability of the midlatitude eddy-driven jet. It is demonstrated that all three sources of jet movement produce a similar change in Rossby wave breaking frequency per degree of jet shift. Hence, it is difficult (if not impossible) to isolate the ultimate cause behind the shift in Rossby wave breaking in response to the two external forcings.

## 1. Introduction

The mutual interaction between storm tracks and the zonal-mean flow in the midlatitudes has been the focus of intense research during the last few decades. As storms grow and reach their maximum amplitude, they feed back onto the large-scale circulation and modify the large-scale winds through the divergence of their momentum fluxes (Held 1975; Simmons and Hoskins 1978; Edmon et al. 1980; Hoskins et al. 1983) and thus participate in the formation of the large-scale flow (Yu and Hartmann 1993; Branstator 1995; Akahori and Yoden 1997; Feldstein and Lee 1998; Robinson 1996; Lorenz and Hartmann 2001). Much of this interaction occurs via wave-breaking processes (Hartmann 1995; Benedict et al. 2004; Rivière and Orlanski 2007; Martius et al. 2007; Strong and Magnusdottir 2008; Woollings et al. 2008). Specifically, wave breaking has been linked to the different phases of the North Atlantic Oscillation (Franzke et al. 2004;

Benedict et al. 2004; Rivière and Orlanski 2007), the Pacific–North American pattern (Martius et al. 2007; Franzke et al. 2011), and hemispheric variations of the large-scale flow such as those diagnosed by the zonal index (e.g., Hartmann 1995; Akahori and Yoden 1997; Gong et al. 2010; Wang and Magnusdottir 2011). Changes in wave breaking have been associated with climate change and stratospheric variability (Wittman et al. 2004; Kunz et al. 2009; Rivière 2011; Barnes and Hartmann 2012; Ndarana et al. 2012; Barnes and Polvani 2013; Lu et al. 2014). Furthermore, Rossby wave breaking (RWB) is directly associated with stratosphere–troposphere exchange (Sprenger et al. 2007). Therefore, it is crucial to understand its distribution.

Many mechanisms have been provided to explain how the midlatitude jet responds to external forcings, and some of those mechanisms involve changes in RWB frequency, morphology, or distribution. For example, changes in wave breaking have been identified as the cause of meridional shifts of the tropospheric jet in response to the polar vortex (Wittman et al. 2007; Kunz et al. 2009) and to strengthened upper-tropospheric baroclinicity in response to global warming (Rivière 2009, 2011; Wilcox et al. 2012).

---

*Corresponding author address:* Chaim I. Garfinkel, Earth Science Institute, Hebrew University, Jerusalem, Israel.  
E-mail: chaim.garfinkel@mail.huji.ac.il

The primary goal of this paper is to assess whether such processes can be identified and isolated in a model in which unforced, stochastic variability is present. Specifically, we quantitatively assess the linkage between anomalies in the meridional position of the jet (i.e., jet latitude) and anomalies in RWB distribution for three unique processes whereby RWB and the jet latitude changes: a baroclinic forcing that resembles certain aspects of observed climate change, internal variability, and the imposition of a polar vortex. We thereby gauge the tightness of the coupling between jet latitude and RWB and specifically assess to what degree changes in RWB distribution can be isolated from changes in jet latitude.

As a first step toward understanding changes in RWB in nature, we focus here on a simplified dry GCM in which stochastic, unforced variability in jet latitude exists yet jet latitude is influenced by external forcings. After introducing the model and our RWB detection algorithm, we focus on the climatological distribution of RWB as a baroclinic forcing modifies the baseline jet latitude. We then consider whether these changes in RWB due to a baroclinic forcing can explain how RWB changes due to internal, unforced variability of the jet and due to the imposition of a strong stratospheric polar vortex. We will demonstrate that, for three difference sources of a shift in jet latitude, the RWB anomaly associated with that jet shift is identical: the jet shift and the accompanying RWB changes are inextricably tied together. Stated another way, these results suggest that the change in RWB per degree latitude does not depend on the time scale of the jet shift: both internal variability (in which the characteristic time scale for the jet shift is several weeks) and externally forced, long-time-scale variability lead to identical RWB anomalies. While this does not necessarily disprove any specific mechanism that connects an external forcing directly to RWB, it does suggest that it will be very difficult to provide evidence for these mechanisms in a data source in which stochastic variability of jet latitude is present.

## 2. Data and methods

### a. The idealized dry model

The Geophysical Fluid Dynamics Laboratory (GFDL) spectral atmospheric dynamical core is used to isolate the relationship between the tropospheric jet and RWB. A full description of the experiments can be found in Garfinkel et al. (2013), but for completeness we briefly describe the experiments. In the troposphere, the model parameterizations follow Held and Suarez (1994, hereafter HS94), except for the following modifications: HS94 specify the tropospheric temperature profile as

TABLE 1. Different experiments performed for understanding the dependence of Rossby wave breaking on jet latitude. For each tropospheric parameter setting, an integration with a strong vortex and an integration with no vortex (i.e.,  $\gamma = 0$  and  $\gamma = 6$ ). Note that jet latitude increases along with  $A$  and  $B$ .

Dry model tropospheric parameter settings			
Experiment	$A$	$B$	$P(\phi)$ in Eq. (2)
J30	0	0	—
	−10	0	$\sin(4\phi - 45)$
	−5	0	$\sin(4\phi - 45)$
	5	0	$\sin(4\phi - 45)$
	10	0	$\sin(4\phi - 45)$
	5	0	$\sin[4(\phi - 45)]$
J40	10	0	$\sin[4(\phi - 45)]$
	5	4	$\sin[4(\phi - 45)]$
	5	8	$\sin[4(\phi - 45)]$
	5	12	$\sin[4(\phi - 45)]$
	5	16	$\sin[4(\phi - 45)]$
J50	5	20	$\sin[4(\phi - 45)]$

$$T_{\text{eq}}^{\text{trop}}(p, \phi) = \max(200 \text{ K}, (T_0 - \delta T_{\text{HS94}}) \frac{p}{p_0}^{\kappa}), \quad (1)$$

where  $\delta T_{\text{HS94}} = (\Delta T)_y \sin^2 \phi + (\Delta T)_z \log(p/p_0) \cos^2 \phi$ ,  $T_0 = 315 \text{ K}$ ,  $p_0 = 1000 \text{ hPa}$ ,  $(\Delta T)_y = 60 \text{ K}$ , and  $(\Delta T)_z = 10 \text{ K}$ , where we use the same notation as HS94. To vary the climatological position of the jet, two additional terms are added onto  $\delta T_{\text{HS94}}$  to form  $\delta T_{\text{new}}$ , which replaces  $\delta T_{\text{HS94}}$  in Eq. (1),

$$\begin{aligned} \delta T_{\text{new}} = & \delta T_{\text{HS94}} + A \cos[2(\phi - 45)]P(\phi) \\ & + B \cos[2(\phi - 45)] \sin[3(\phi - 60)] \\ & \times \left\{ \exp \left[ -\frac{(\phi - 15)^2}{2(15^2)} \right] + \exp \left[ -\frac{(\phi + 15)^2}{2(15^2)} \right] \right\}, \end{aligned} \quad (2)$$

where  $P(\phi) = \sin[4(\phi - 45)]$  or  $P(\phi) = \sin(4\phi - 45)$  (depending on the case). Note that increasing  $A$  and  $B$  shift the baroclinicity poleward. By modifying the values of  $A$  and  $B$  and the form of  $P(\phi)$ , the tropospheric baroclinicity and thus the climatological position of the jet can be shifted meridionally. Each unique tropospheric configuration [unique combination of  $A$ ,  $B$ , and  $P(\phi)$ ] will be referred to as an experiment. Table 1 lists the key parameterizations, including the values of  $A$ ,  $B$ , and  $P(\phi)$ , for each experiment. The experiment denoted J30 (i.e., jet near  $30^\circ$ ) is identical to cases 7 and 10 of Gerber and Polvani (2009), except that we set the asymmetry factor between the two hemispheres [ $\epsilon$  in Eq. (A4) of Polvani and Kushner 2002] to 0 so that the equator-to-pole temperature difference is constant in both hemispheres. Two additional experiments are denoted J40 and J50 (i.e., jet near  $40^\circ$  and  $50^\circ$ ), corresponding to the approximate jet

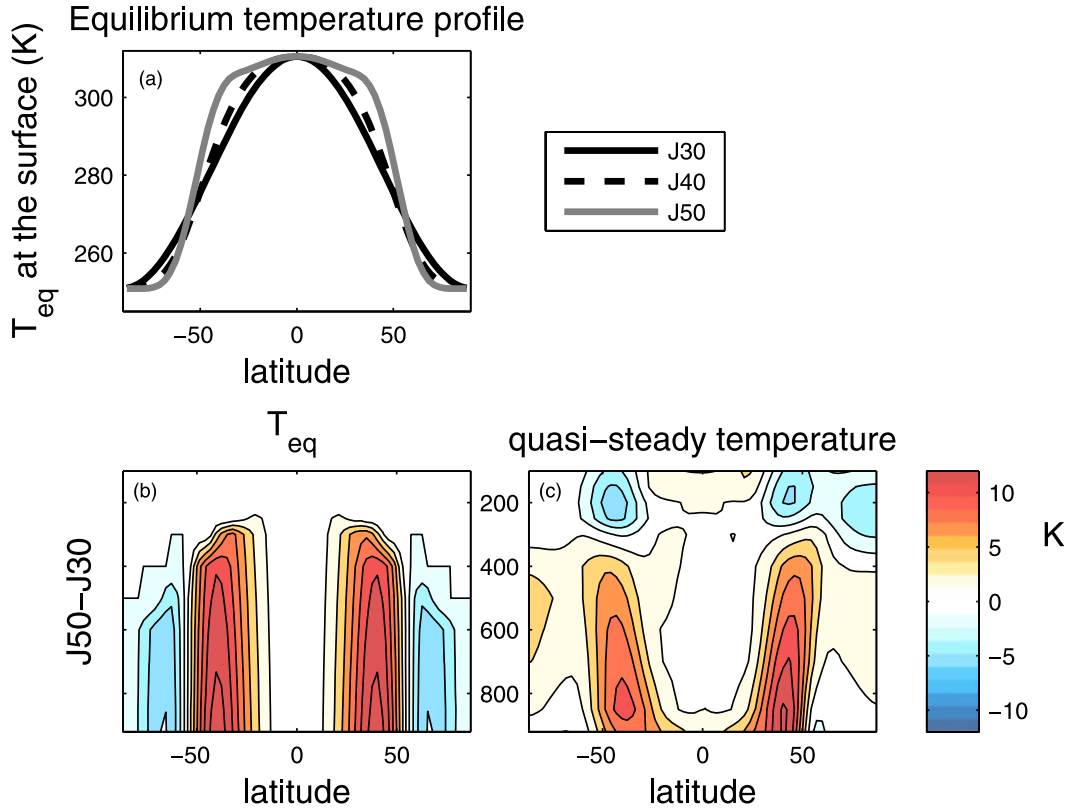


FIG. 1. Surface temperature toward which the model is relaxed for the J30, J40, and J50 cases. In (b) and (c) the contour interval is 2 K.

latitude of observed wintertime jets in the North Atlantic and Southern Hemisphere (SH). The net effect of  $A$ ,  $B$ , and  $P(\phi)$  on the total baroclinicity is demonstrated graphically in Fig. 1a, which shows the surface equilibrium temperature profile for the J30, J40, and J50 cases. The vertical structure of the change in  $\delta T_{\text{new}}$  between the J50 and J30 experiments is shown in Fig. 1b. The temperature difference once the experiments have reached quasi equilibrium (after the spinup period has been discarded) is shown in Fig. 1c. In the quasi steady state, the biggest impact of the change in baroclinicity is to warm the midlatitude troposphere. While the temperature change certainly differs from that forced by climate change in some regions, it does resemble the recent warming as observed by satellites in one crucial manner: the warming is mostly in midlatitudes as compared to the tropics (Fu et al. 2006; Allen et al. 2012; Tandon et al. 2013). Specifically, the temperature profile bears some resemblance to that shown for the Phi35–20 case in Figs. 1 and 2 in Tandon et al. (2013); this midlatitude warming has been found to be important in driving the poleward jet shift in response to climate change (Tandon et al. 2013; Ceppi et al. 2014). Finally, note that the equator-to-pole temperature difference does not change with  $A$ ,  $B$ , or  $P(\phi)$ . Garfinkel

et al. (2013) showed that this leads to heat fluxes and maximum jet speeds that are nearly equal in strength among all the integrations, two traits we consider desirable because the strength of the jet can affect the RWB distribution independently of jet latitude.

A more realistic stratosphere is created following Polvani and Kushner (2002). Above 100 hPa, the equilibrium temperature profile is given by  $T_{\text{eq}}^{\text{strat}}(p, \phi) = [1 - W(\phi)]T_{\text{US}}(p) + W(\phi)T_{\text{PV}}(p)$ , where  $T_{\text{US}}$  is the U.S. standard temperature;

$$T_{\text{PV}}(p) = T_{\text{US}}(p_T) \frac{p}{p_T}^{R\gamma/g} \quad (3)$$

is the temperature of an atmosphere with a constant lapse rate  $\gamma$  ( $\text{K km}^{-1}$ ); and  $W(\phi)$  is a weight function that confines the cooling over the pole,

$$W(\phi) = \frac{1}{2} \left[ 1 - \tanh \left( \frac{\phi - \phi_0}{\delta\phi} \right) \right], \quad (4)$$

with  $\phi_0 = 50$  and  $\delta\phi = 10$ . By modifying the values of  $\gamma$ , the strength of the polar vortex can be controlled. For

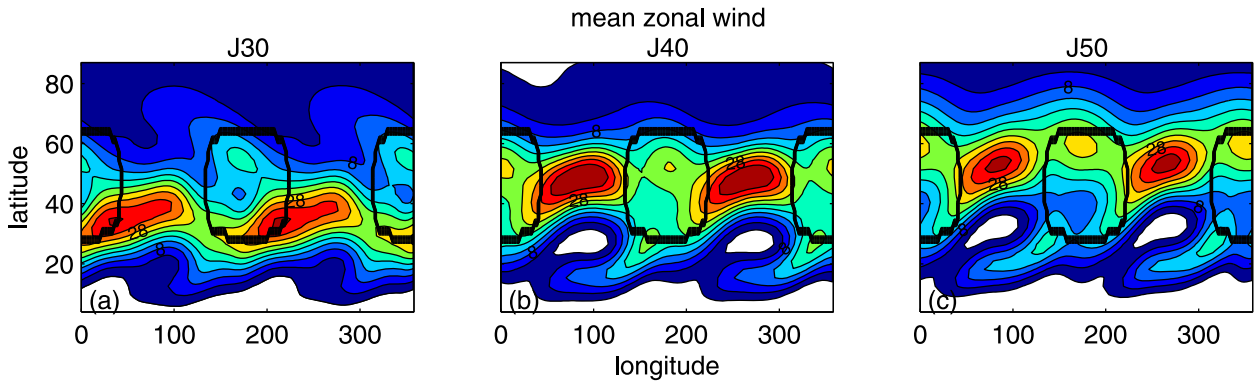


FIG. 2. Climatological 250-hPa zonal wind for the J30, J40, and J50 cases, as a function of latitude and longitude. The contour interval is  $4 \text{ m s}^{-1}$ , and easterlies are shaded white. The location of the peak topography is indicated in black.

each experiment, a pair of integrations is performed: one with no vortex and one with a strong stratospheric polar vortex ( $\gamma = 0$  and  $\gamma = 6$ ).

Wavenumber-2 topography that is 6 km high from peak to trough is added in the hemisphere where the stratospheric vortex is imposed following Gerber and Polvani (2009) in order to excite more realistic variability and to help eliminate regime behavior in the troposphere. All figures and discussion in this paper are for the hemisphere with the topography and vortex.

The sigma vertical coordinate has forty vertical levels defined as in Polvani and Kushner (2002). Model output data on sigma levels are interpolated to pressure levels before any analysis is performed. The horizontal resolution is T42. The  $\nabla^8$  hyperdiffusion in the model selectively damps the smallest-scale spherical harmonic at a time scale of 0.1 days. The model output is sampled daily. After discarding a 400-day spinup period, we examine 5100 days of model output for each experiment (note that some experiments extend for much longer; Garfinkel et al. 2013).

In summary, our approach is to create a continuum of experiments in which the tropospheric baroclinic forcing and stratospheric polar vortex gradually moves the jet from near  $27.5^\circ$  to near  $54^\circ$ . The key parameters of the study are  $A$  and  $B$ , which vary the tropospheric temperature gradient, and  $\gamma$ , which determines the strength of the polar vortex. We then analyze the subsequent RWB frequency.

### b. Control run jets

We introduce the ensemble of basic states in which jet latitude varies from near  $27.5^\circ$  to near  $54^\circ$  in this section. Figure 2 shows the upper-tropospheric time-mean zonal wind as a function of latitude and longitude, and the location of the topographic features, for the J30, J40, and J50 cases. As discussed in Garfinkel et al. (2013), the jet peak is around  $30 \text{ m s}^{-1}$  in all three cases and near the latitude indicated by their name. The wavenumber-2

topography imposed leads to a zonally asymmetric jet whereby there is a relative maximum in zonal wind near  $90^\circ$  and  $270^\circ\text{E}$  in the extratropics downstream of the topography.

In all cases, the midlatitude jet is eddy driven. High-frequency eddy momentum flux convergence (EMFC;  $-(1/\cos^2\phi)(\partial \cos^2\phi \langle u'_{hi} v'_{hi} \rangle / \partial \phi)$ ) maximizes near the latitude of the jet in all cases (Fig. 3a), while eddies remove momentum from the flanks of the jet. See Garfinkel et al. (2013) for additional diagnostics for the mean state in each experiment.

### c. The methodology for identifying RWB

We now introduce the methodology used for tracking the distribution of RWB. The methodology for identifying RWB relies on overturning absolute vorticity contours ( $\eta = f + \zeta$ , where  $f$  is the Coriolis parameter) as in Barnes and Hartmann (2012). We look for wave breaking on 18 absolute vorticity contours  $\pm[1, 2.75, 4.5, 6.25, 8, 9.75, 11.5, 13.25, 14.75] \times 10^{-5} \text{ s}^{-1}$ . For reference, Fig. 4 shows the climatological location of these contours in the J30 case as compared to zonal-mean zonal wind and eddy momentum flux convergence. We have examined the RWB distribution upon removing some of these contours, and we find quantitatively similar results; the selected contours are sufficient to record RWB activity throughout the globe.

The specific procedure is as follows: We first smooth the absolute vorticity before the wave-breaking algorithm is applied to ensure that only large-scale overturning—and not small-scale perturbations in the field—are included as a wave breaking event. This is accomplished by only including the first 11 Fourier harmonics of zonal variability of the field. Each day, we search for large-scale wave breaking by searching for regions of overturning of each of the 18 absolute vorticity contours. The algorithm identifies wave breaking events by first identifying circumpolar closed contours. The algorithm then searches

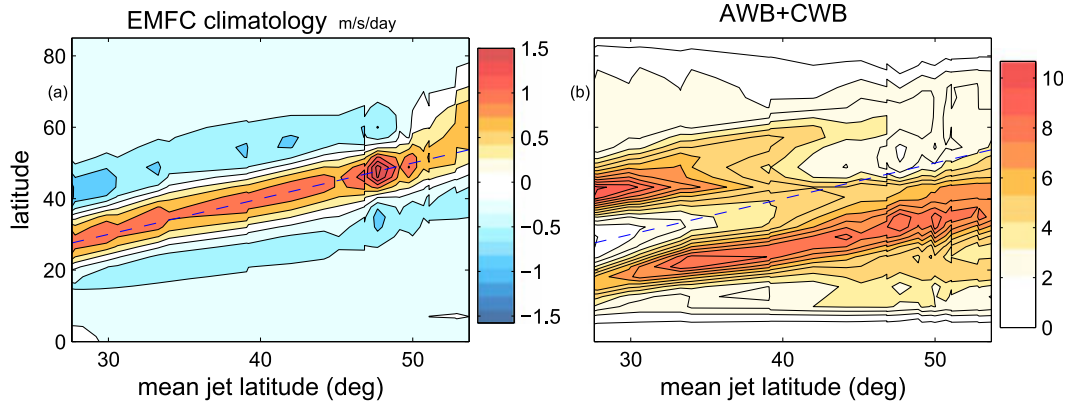


FIG. 3. (a) Eddy momentum flux convergence for all of the dry model experiments. Units of EMFC are  $\text{m s}^{-1} \text{day}^{-1}$   $[-(1/a \cos^2 \phi)(\partial \cos^2 \phi(\overline{u'v'})/\partial \phi)]$ . (b) Rossby wave breaking frequency (per day) as a function of latitude (i.e., sum over longitude) for each tropospheric forcing. The dashed line denotes the one-to-one line and thus the position of the mean jet core.

for meridians which intersect the contour at least three times. When this occurs, we call these three intersecting grid points “overturning points” for this contour and meridian, and adjacent overturning points are grouped to form an “overturning event.” To ensure that subsynoptic variability has been removed, the minimum longitudinal width of an overturning event is set to  $5^\circ$  as in Barnes and Hartmann (2012). This method is applied daily to the aforementioned contour values with all resulting overturning groups saved. The grid points included in the overturning event define the “overturning region,” and the center of the overturning region is defined as the geographic centroid of the event. The center, latitudinal and longitudinal bounds, potential vorticity, and momentum flux of the overturning events are archived and form the wave-breaking climatology.

Thorncroft et al. (1993) gave a detailed description of two life cycles, life cycle 1 [LC1; anticyclonic wave breaking (AWB)] and life cycle 2 [LC2; cyclonic wave breaking (CWB)], in baroclinic life cycle experiments. In the final stage of the anticyclonic life cycle (LC1), the form of the upper-level wave elongates in the northeast–southwest (NE–SW) direction in the Northern Hemisphere, and often it breaks up into upper-level cutoff vortices (Thorncroft et al. 1993). During the cyclonic life cycle (LC2), in contrast, the disturbance wraps up cyclonically. The life cycles differ significantly not only in terms of their upper-level morphology, but also in the momentum forcing on the mean flow: cyclonic wave breaking events are associated with poleward fluxes of wave activity, and anticyclonic events are associated with equatorward fluxes (e.g., Esler and Haynes 1999).

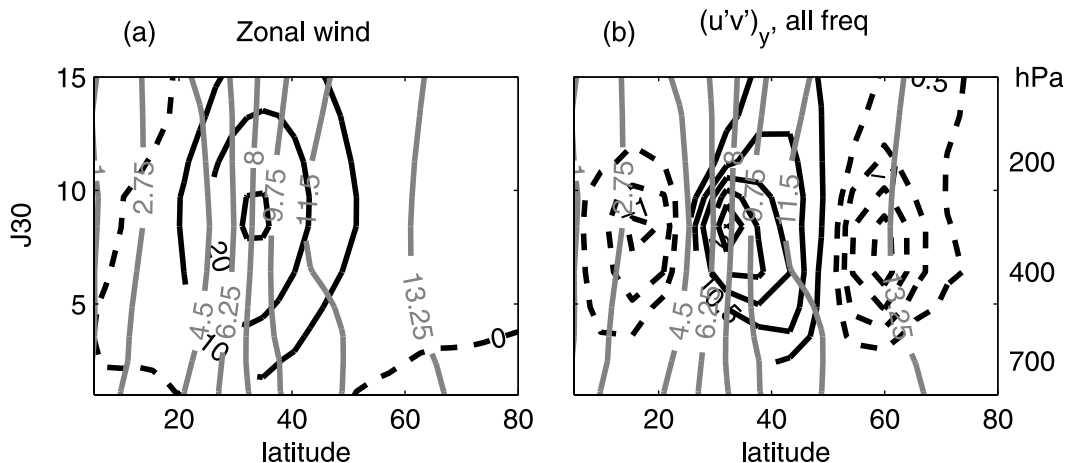


FIG. 4. Latitude–height cross section of (left) zonal-mean zonal wind and (right) total EMFC in J30. Units of EMFC are  $\text{m s}^{-1} \text{day}^{-1}$   $[-(1/a \cos^2 \phi)(\partial \cos^2 \phi(\overline{u'v'})/\partial \phi)]$ . Gray lines are the absolute vorticity  $(\zeta + f) = [1, 2.75, 4.5, 6.25, 8, 9.75, 11.5, 13.25, 14.75] \times 10^{-5} \text{s}^{-1}$  contours, the contours on which we identify RWB events. The contour interval is (a)  $10 \text{ m s}^{-1}$ , where the zero line is dashed, and (b)  $0.5 \text{ m}^2 \text{ s}^{-2}$ , where the zero contour is omitted.

Hence, the results presented here differentiate between wave breaking events in which the overturning occurs cyclonically and those in which the overturning occurs anticyclonically. Two methodologies were explored for this: In the first, the eddy momentum flux ( $u'v'$ ) was computed in the overturning region (as in [Ndarana and Waugh 2011](#)). In the second, the eddy momentum flux was computed by analyzing the morphology of the wave breaking (specifically by comparing the change in absolute vorticity in the northwest/southeast direction with the change in the northeast/southwest direction at the centroid). Both definitions lead to quantitatively similar climatologies; for brevity, we show the results for the morphology definition only. Sensitivity to removing small and/or weak events will be discussed in [section 3a](#). The morphology of CWB can be seen in [Fig. 2a](#) near 65°N at the longitude of the jet core, while the morphology of AWB can be seen in [Fig. 2c](#) near 35°N at the longitude of the jet core.

We focus on RWB at the 250-hPa level, though results are similar at adjacent levels. If we focus slightly lower in the atmosphere, subpolar CWB increases, while, if we focus slightly higher in the troposphere, subtropical AWB increases (not shown). These changes with height are consistent with the sloping of the tropopause toward the pole and with [Martius et al. \(2007\)](#). In addition, we have performed our analysis using overturning potential vorticity contours as well, and results are similar [the merits of focusing on absolute vorticity, as opposed to potential vorticity, are discussed in [Barnes and Hartmann \(2012\)](#)].

Thus far, the RWB database includes events that might be considered duplicates. For certain applications (e.g., How many RWB events are there per year at a given location?), it is of paramount importance to remove such possible duplicates. However, the primary interest of this paper is in how RWB frequency changes as the jet moves (and not in the absolute number of events), and thus we focus on the database which includes (potentially) duplicate events. In addition, our attention is focused mainly on the location of the RWB centroid (as opposed to the total area encompassed by a RWB event), and RWB events on different absolute vorticity surfaces cannot share the same centroid. Finally, the dry model appears to simulate more RWB events than the National Aeronautics and Space Administration (NASA) Modern-Era Retrospective Analysis for Research and Applications (MERRA; [Rienecker et al. 2011](#)) reanalysis as discussed in the [appendix](#), and thus the absolute number of RWB events as simulated by the dry model is likely not relevant to nature. We therefore do not quantitatively compare the absolute RWB frequency to that in any other study.

Nevertheless, we assess the sensitivity of our results to removing duplicate events in select figures below as

follows: The list of overturning events on any of the contours is concatenated. Overturning events in which the centroids lie within 3000 km of each other in a great circle distance are considered part of the same event. As a single wave breaking event often lasts more than 1 day, we ensure that we do not double count the same wave breaking event across multiple days as follows: Unique events must be separated by 3000 km in a great circle distance for 2 days following the first day. Otherwise, the first day of the group is defined as the “onset day” and the overturning event during the following 2 days is considered as a duplicate. The net effect of the procedure described in this paragraph is that out of every 25 RWB events originally identified, approximately 24 are identified as duplicates and are removed. Note that the number of events removed and thus the absolute frequency are highly sensitive to the aforementioned criteria (e.g., 3000 km), and there is no rigorous way of setting these parameters. In addition, there is more intraensemble noise when we consider unique events only. Instead, our primary focus in this article is on the relative frequency of RWB as the latitude of the jet changes.

### 3. Effect of the baroclinic forcing on RWB distribution

The RWB frequency as a function of jet position and latitude is shown in [Fig. 3b](#). For each jet position, there are at least two local maxima in RWB frequency. The first local maximum occurs on the equatorward flank of the jet, and the second local maximum occurs on the poleward flank of the jet. There is a relative minimum in RWB frequency near the latitude of the jet itself. For jets poleward of 45°, there is a third maximum in the subtropics on the equatorward flank of the jet. All of these features move poleward as the jet position is farther poleward, except for the maxima in the subtropics for jets poleward of 45°. These maxima in RWB provide the momentum flux (shown in [Fig. 3a](#)) that drives the eddy-driven jet. [Figure 5a](#) shows the climatological high-frequency EMFC for experiments with jet latitude near 40° (results are insensitive to the experiment chosen) separated into RWB dates/regions and RWB-less dates/regions. The high-frequency EMFC that occurs in RWB dates/regions dominates the total high-frequency EMFC, while high-frequency EMFC that occurs in no-RWB dates/regions is important only on the flanks of the jet.

The maxima in RWB frequency on the equatorward flank of the jet is associated mainly with AWB ([Fig. 6a](#)), while the maxima on the poleward flank of the jet is associated mainly with CWB [[Fig. 6b](#); consistent with [Akahori and Yoden \(1997\)](#), [Hartmann \(1995\)](#), and

## Isolating RWB gridpoints from no-RWB gridpoints

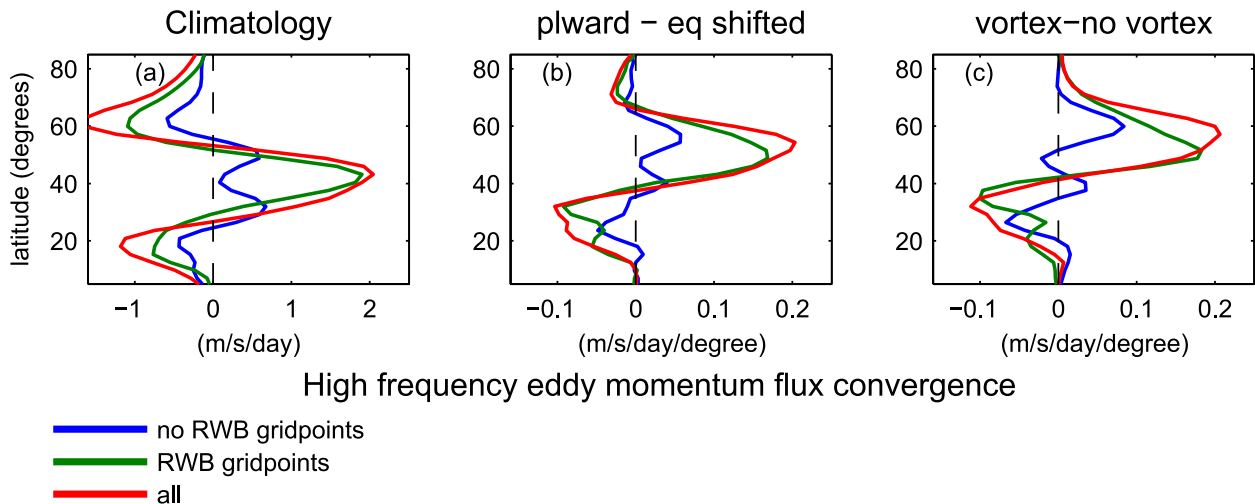


FIG. 5. Contribution of wave breaking to the high-frequency EMFC. We average the experiments in which the change in jet latitude due to a vortex exceeds  $5^\circ$  (which naturally selects jets near  $40^\circ$ ; Garfinkel et al. 2013). (a) The climatological high-frequency EMFC associated with grid points in which a RWB event has been identified and in grid points in which no RWB event has been identified. (b) The change in high-frequency EMFC per degree latitude of jet shift associated with internal variability of the jet, broken down into regions in which a RWB event has been identified and regions in which no RWB event has been identified. (c) As in (b), but for the response to imposing a stratospheric polar vortex. The separation into RWB and no-RWB regions is as described in section 2c. The change in EMFC is quantitatively similar for both forced and unforced variability after we normalize by the magnitude of the jet shift and is dominated by the change in EMFC in RWB regions/dates.

others]. These maxima provide the momentum flux that drives the eddy-driven jet, as AWB events flux momentum poleward while CWB events flux momentum equatorward. All of these features are consistent with those shown for comprehensive models and reanalysis data in Barnes and Hartmann (2012) and Barnes and Polvani (2013).

### a. Sensitivity to excluding weak RWB events

To produce a climatology of RWB, several subjective choices must be made regarding what events are categorized as sufficiently strong and/or distinct. We therefore investigate whether our climatology of RWB is sensitive to these choices. We consider four unique ways of evaluating weak RWB events. For each of the four, the thresholds are chosen so that approximately 70% of the RWB events are discarded. Overall, this section will show that, while the overall pattern of the distribution of RWB with latitude appears robust, many of the details are sensitive to the exclusion of marginal RWB events.

First, we consider RWB events in which the momentum flux anomaly averaged in the RWB region exceeds  $25 \text{ m}^2 \text{ s}^{-2}$  (Figs. 6c,d). The local maximum of CWB frequency on the equatorward flank of the jet (which counters the time-mean momentum flux shown in Fig. 3a and thus weakens the jet) is now no longer as present (Fig. 6c); similarly, the local maximum of AWB frequency on the poleward flank of the jet (which counters the time-mean

momentum flux shown in Fig. 3a and thus also weakens the jet) is no longer present (Fig. 6d). In other words, the strongest 30% of RWB events tend to drive the eddy-driven jet at the jet core exclusively. Finally, the maximum in RWB frequency in the subtropics now no longer appears; these subtropical RWB events are weak.

Second, we only consider RWB events in which the positive absolute vorticity anomaly in the RWB region exceeds  $1.75 \times 10^{-5} \text{ s}^{-1}$  and thus isolate the RWB events with large circulation anomalies. These RWB events have a large line integral of anomalous vorticity surrounding the wave breaking, if we neglect discretization effects. The distribution of RWB frequency is shown in Figs. 6e,f. Results are generally similar to those shown in Figs. 6c,d: strong AWB events occur predominantly on the equatorward flank of the jet, while strong CWB events occur predominantly on the poleward flank of the jet.

Next, we only consider RWB events in which the overturning region exceeds  $1.6 \times 10^5 \text{ km}^2$  in areal extent. The distribution of RWB frequency is shown in Figs. 6g,h. More large AWB events occur on the poleward flank of the jet and more large CWB events occur on the equatorward flank of the jet as compared to Figs. 6c,d. In other words, the distribution more closely resembles that shown before any events are removed. However, the subtropical maximum is still no longer present; the subtropical RWB events are both weak and small.

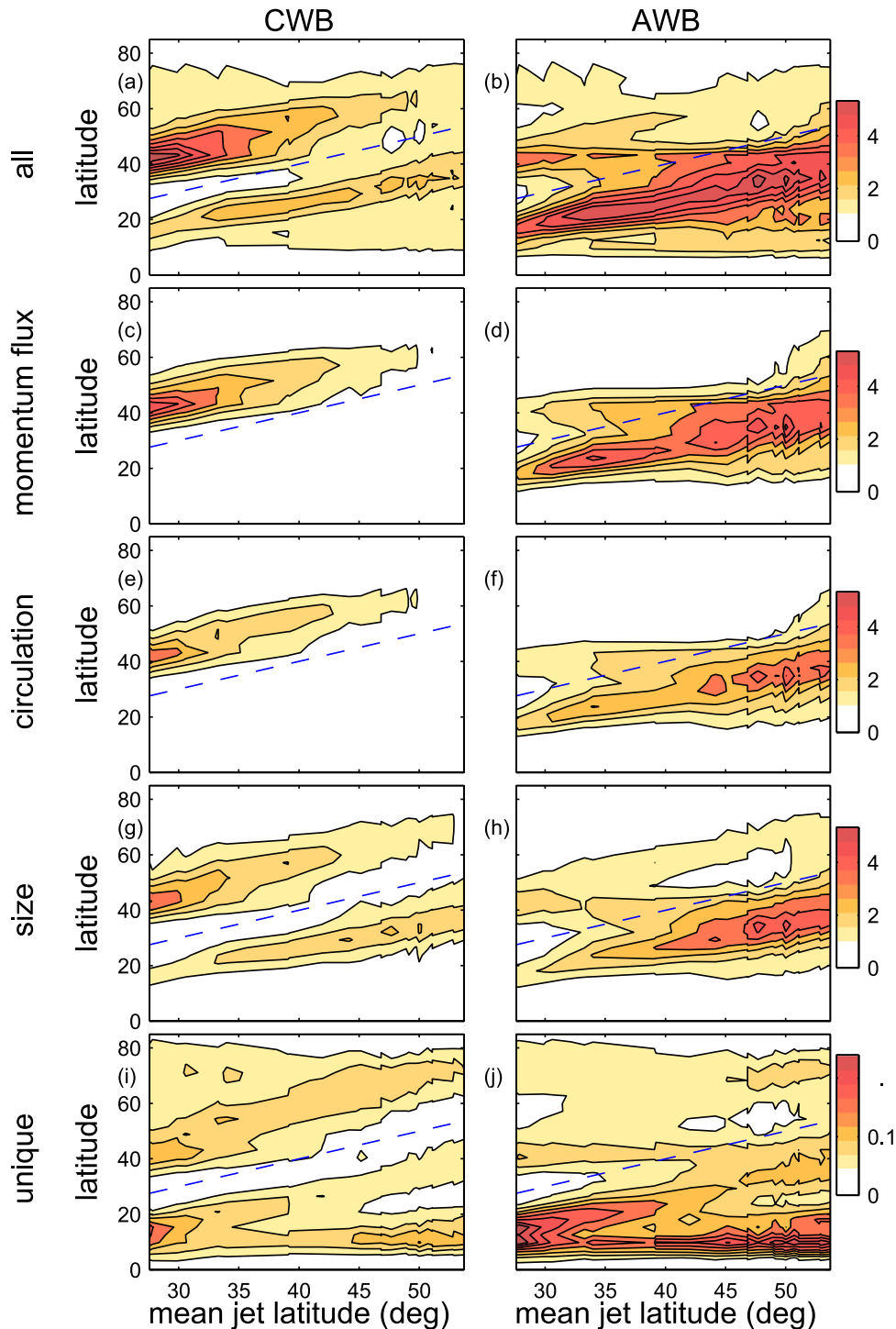


FIG. 6. Rossby wave breaking frequency (per day) as a function of latitude for each tropospheric forcing: (a) total (zonal sum) of CWB frequency and (b) total (zonal sum) of AWB frequency. Sensitivity of cyclonic wave-breaking and anticyclonic wave-breaking frequency to including only the strong events, as a function of latitude: (c),(d) RWB in which the average  $u'v'$  anomaly in the RWB region exceeds  $25 \text{ m}^2 \text{ s}^{-2}$ ; (e),(f) RWB in which the average absolute vorticity anomaly in the RWB region exceeds  $1.75 \times 10^{-5} \text{ s}^{-1}$ ; (g),(h) RWB events larger than  $1.6 \times 10^5 \text{ km}^2$ ; and (i),(j) RWB events that are unique. The dashed line denotes the one-to-one line and thus the position of the mean jet core. The criteria for (c)–(f) are chosen so that approximately 70% of the RWB events are discarded for each of the four cases.

Finally, we consider the RWB frequency when we remove duplicate events as described in section 2c (Figs. 6i,j). The distribution of RWB with latitude closely resembles the original distribution in which no attempt is made to remove duplicate events. The main difference is that the subtropical maximum is now stronger. However, when we exclude duplicate and weak RWB events (as defined by the momentum flux anomaly or the circulation anomaly in the RWB region), the subtropical maxima in RWB frequency is no longer present (not shown). In other words, the RWB events that occur in the subtropics tend to be weaker and are associated with weak momentum fluxes. In summary, the two maxima in RWB distribution near the jet flanks are robust to excluding weak and moderate events, but the subtropical maxima is not.

*b. How does wave breaking change as the baroclinic forcing moves poleward?*

We now discuss how wave breaking changes as the baroclinic forcing moves poleward. We first focus on wave breaking summed over the entire hemisphere, and then we restrict our focus to the region close to the jet core. If we focus on the entire hemisphere, there is a monotonic reduction in CWB frequency as the baroclinic forcing (and hence the jet) moves poleward (Fig. 7a), consistent with Barnes and Hartmann (2012), while AWB frequency monotonically increases as the jet is forced farther poleward (Fig. 7b). When we sum over both types, we find that total RWB frequency increases as the baroclinic forcing moves poleward, but the magnitude of the change is less than a third of the change in AWB or CWB frequency. Hence, there is substantial cancellation between these two effects. The behavior of RWB frequency in state-of-the-art climate models (phase 5 of the Coupled Model Intercomparison Project) resembles that shown here (Barnes and Polvani 2013, their Fig. 10). In contrast, AWB frequency decreases as the jet is found closer to the pole in a barotropic model (Barnes and Hartmann 2012, their Fig. 6a). Future work is needed to understand the behavior of AWB distribution in the barotropic model.

Next, we focus on RWB frequency on either flank of the climatological jet latitude of each integration (results are insensitive to the precise limit chosen; Figs. 7d-i). Equatorward of the jet core, both CWB and AWB frequency tend to increase as the baroclinic forcing moves poleward. The increase in AWB frequency is far larger than the increase in CWB frequency, however, consistent with the poleward shift of the jet itself.

On the poleward flank of the jet, both AWB and CWB frequency decrease as the baroclinic forcing moves poleward [similar to, though weaker than, in Barnes and

Hartmann (2012)]. The role of linear theory, particularly wave reflection as discussed by Lorenz (2014), for this effect is left for future work. The decrease in CWB frequency is twice as strong as the decrease in AWB frequency, however, consistent with the poleward shift of the jet itself. The decrease of CWB frequency with increasing jet latitude on the poleward flank is robust when we exclude weak CWB events (not shown).

The AWB frequency for jets near and poleward of  $50^\circ$  appears to be an exception to the aforementioned results. Namely, AWB frequency no longer increases on the equatorward flank, and slightly increases on the poleward flank, as the jet is forced poleward of  $50^\circ$ . In other words, a kink appears near  $50^\circ$  in Fig. 7h. This phenomenon will be discussed in more detail in section 4c.

Figure 3a suggests that EMFC poleward of the jet approaches zero as the jet approaches the pole. However, this does not imply that RWB frequency approaches zero. Rather, it suggests that the AWB and CWB frequencies are now equal. Specifically, for jets poleward of  $45^\circ$ , the AWB frequency on the poleward flank of the jet is greater than the CWB frequency (Figs. 7g,h), which is consistent with the near-zero EMFC on the poleward jet flank in these cases.

#### 4. Changes in RWB due to internal variability and a stratospheric polar vortex

In this section, we evaluate the changes in RWB frequency associated with internal variability and due to a polar vortex. We then compare the changes in RWB frequency due to these processes to the change in RWB frequency associated with the baroclinic forcing discussed in section 3. We thereby gauge whether the change in RWB frequency due to an external forcing can be separated from the change in RWB frequency due to a jet shift.

*a. How much does RWB frequency change because of internal, unforced jet variability?*

We first discuss how RWB frequency changes because of internal, unforced variability of the jet. Our methodology is as follows. For each 5100-day integration, we composite the 4000 days in which jet latitude differs most strongly from its climatological value (e.g., 2000 poleward-shifted days and 2000 equatorward-shifted days) into a poleward-shifted and an equatorward-shifted composite. We then compare the composites and assess the changes in RWB frequency associated with internal variability. Figures 8a-c summarize the change in RWB distribution in all of the experiments. The pattern of the RWB anomaly tends to have four or five extremes, not just two (Figs. 8a-c). In other words, RWB anomalies

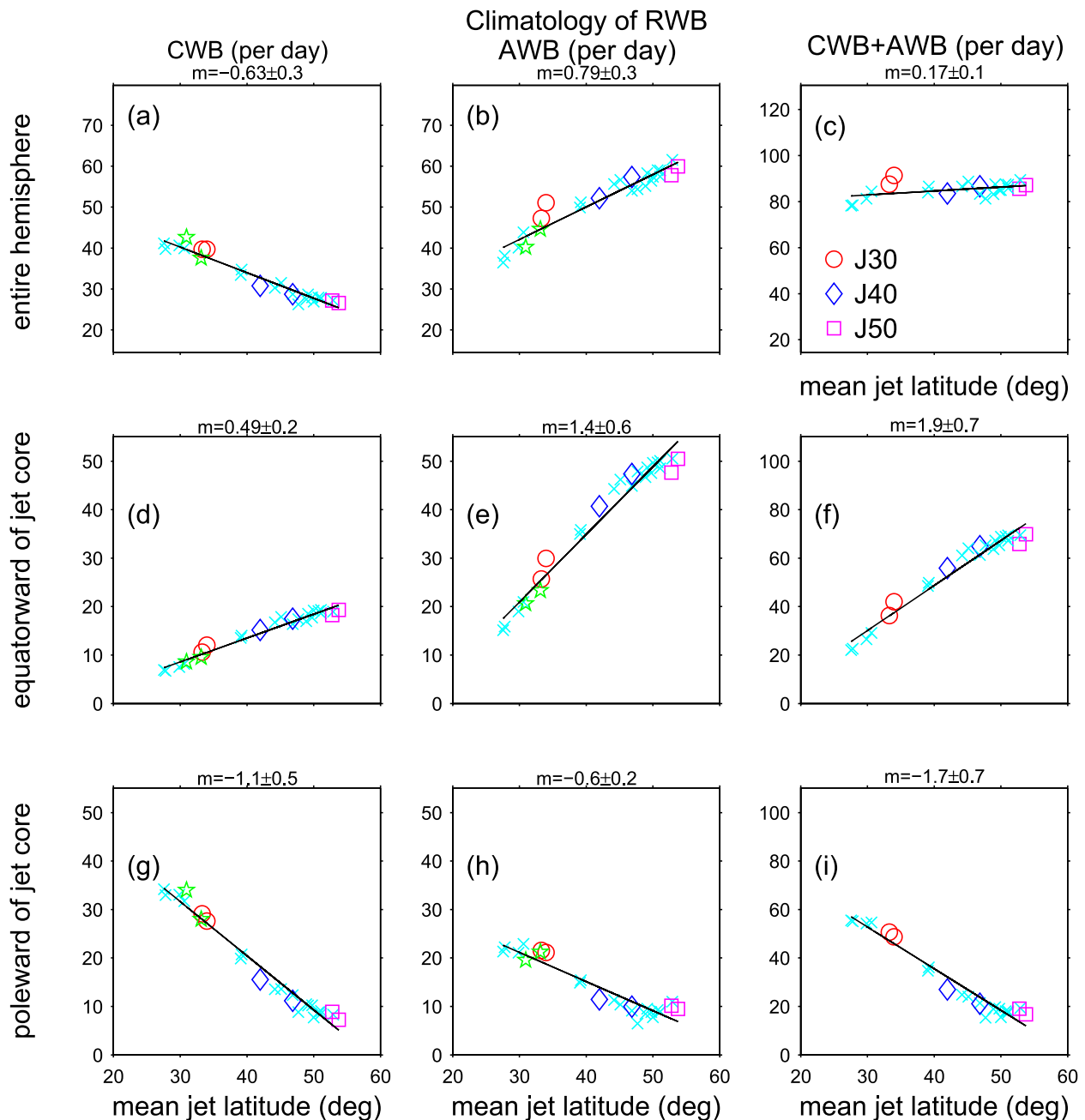


FIG. 7. Scatterplots of Rossby wave breaking in relationship to jet latitude and tropospheric forcing. (a) Total (sum over the entire hemisphere) of CWB frequency. (b) Total (sum over the entire hemisphere) of AWB frequency. (c) Total (sum over the entire hemisphere) of RWB frequency. (d) CWB frequency on the equatorward flank of the climatological jet. (e) Total AWB frequency on the equatorward flank of the climatological jet. (g) CWB frequency on the poleward flank of the climatological jet. (h) AWB frequency on the poleward flank of the climatological jet. A best-fit line is fit for each panel, and the slope of the best-fit line and its 95% uncertainty bounds are listed above the panel. The uncertainty bounds are computed as in [Garfinkel et al. \(2013\)](#). The J30, J40, and J50 cases are as indicated, and all other experiments are represented by a cyan cross.

cannot be accurately summarized as AWB equatorward of the jet and less CWB poleward of the jet. While these additional extremes might not be directly involved in the maintenance of the underlying jet shift, they could be

important for other impacts, such as cutoff lows or stratosphere–troposphere exchange. However, if we restrict our attention to near the jet core or if we focus solely on the strong RWB events (shown in [Figs. 8d,e](#)), we

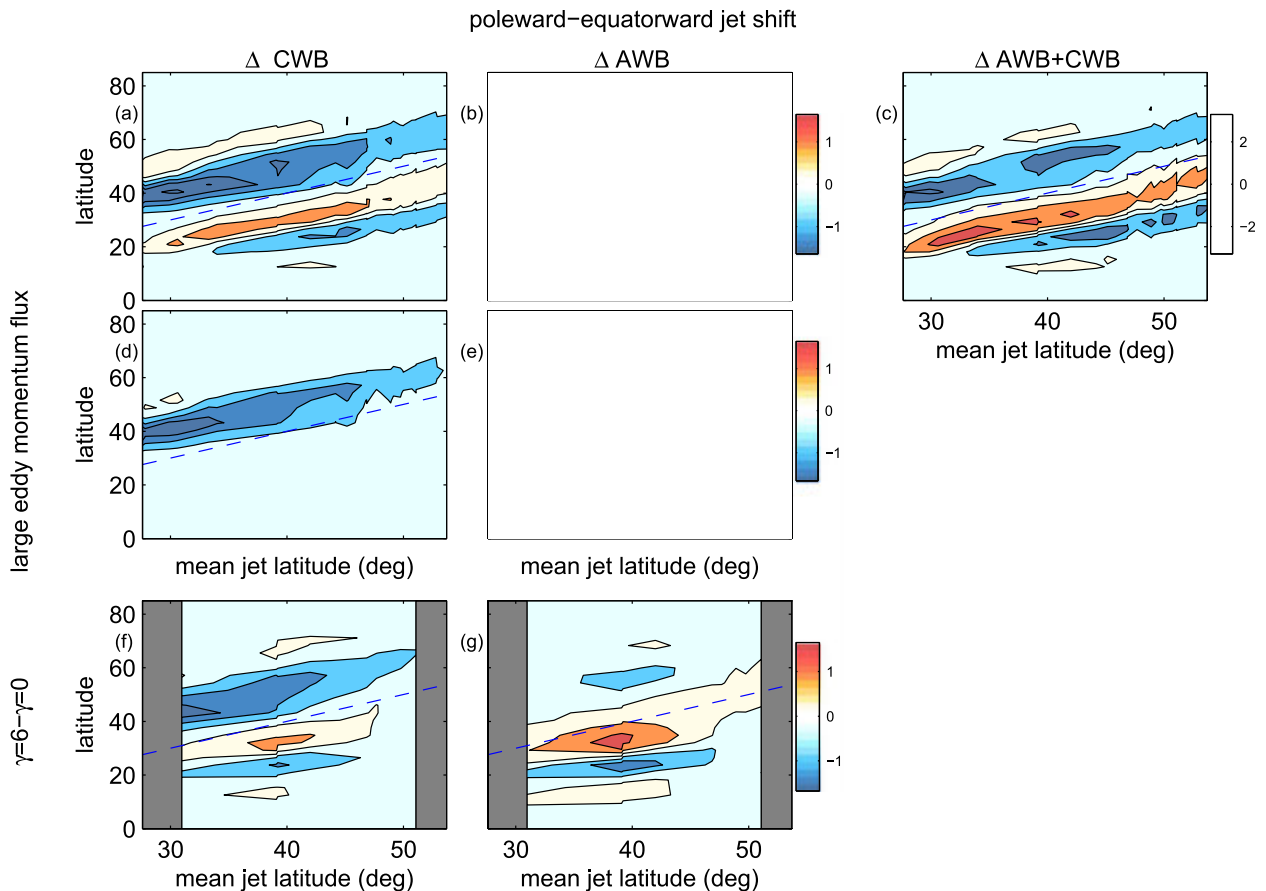


FIG. 8. Difference in Rossby wave breaking frequency between a composite of days in which the jet is poleward shifted and a composite of days in which the jet is equatorward shifted, as a function of latitude for each tropospheric forcing. (a) Total (zonal sum) of CWB frequency. (b) Total (zonal sum) of AWB frequency. (c) Total (zonal sum) of RWB frequency. (d),(e) Sensitivity of cyclonic wave-breaking and anticyclonic wave-breaking frequency to including RWB in which the average  $u'v'$  anomaly in the RWB region exceeds  $25 \text{ m}^2 \text{ s}^{-2}$  only, as in Figs. 6d,e. (f),(g) As in (a),(b), but for the difference in Rossby wave breaking frequency between the integration with a strong vortex ( $\gamma = 6$ ) and a weak vortex ( $\gamma = 0$ ); only cases in which the jet shift because of the vortex exceeds  $1^\circ$  are shown. The dashed line denotes the one-to-one line and thus the position of the mean jet core.

recover the results from Gong et al. (2010) and Wang and Magnustottir (2011) (among others): a poleward shift is associated with more AWB equatorward of the jet and less CWB poleward of the jet.

Figure 9 summarizes the changes in RWB frequency due to internal variability of the jet. For this figure, all of the changes in RWB frequency are normalized by the change of the jet latitude between the poleward-shifted composite and the equatorward-shifted composite, as the magnitude of the jet shift between the composites varies among the experiments performed; therefore, the a priori expectation is that all the points will fall along a line with zero slope. A poleward shift in the jet is associated with less frequent CWB and more frequent AWB (Figs. 9a,b), and the net effect is that total RWB frequency is unchanged (Fig. 9c). These changes are clearer if we focus on either side of the jet core: a poleward shift of the jet is

associated with more RWB (and specifically AWB) equatorward of the jet core and less RWB (specifically CWB) poleward of the jet core.

Finally, the changes in RWB frequency due to internal variability of the jet are similar to those seen in the Southern Hemisphere of MERRA. The change in RWB frequency due to internal variability of the jet in MERRA is denoted by black stars in Fig. 9 [with one star for the pre-ozone-hole era (i.e., before 1985) in those cases in which the pre-ozone-hole era change was not noisy and one star for 1994 and onward]. It is clear that the change in RWB per degree jet shift is indistinguishable in the dry model and in MERRA.

#### b. How does RWB change in the presence of a vortex?

We now discuss the changes in RWB frequency upon imposing a stratospheric polar vortex. Note that we

## Difference in RWB for internal variability of jet

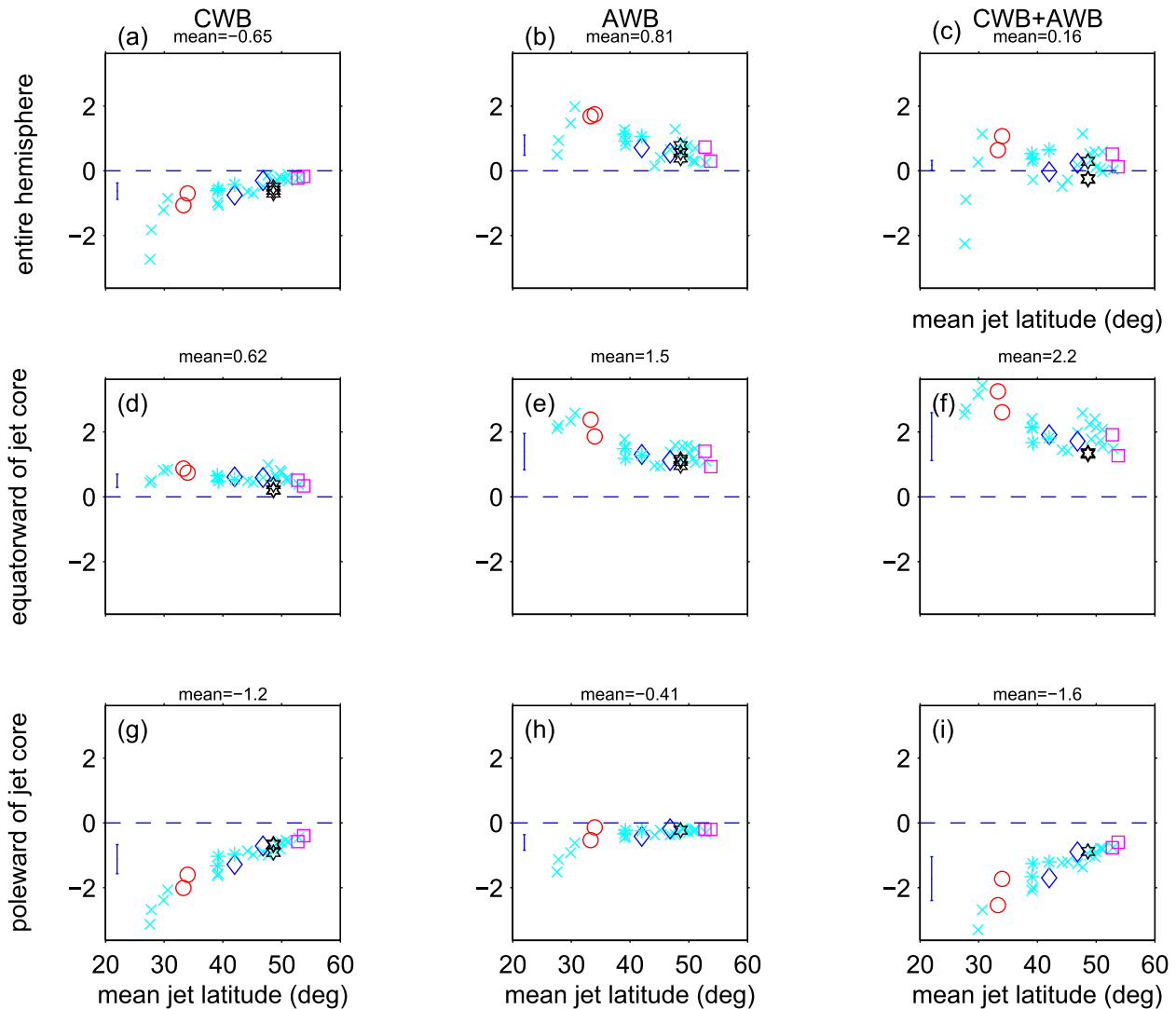


FIG. 9. As in Fig. 7, but for the difference in Rossby wave breaking between equatorward-shifted and poleward-shifted jet time periods. The difference in RWB frequency for the MERRA data is indicated by black stars, and the difference due to imposing a vortex (in the three cases where the jet shift induced by the vortex exceeds  $4^\circ$ ) is shown by cyan asterisks. An error bar on the left side of each panel shows the change in RWB frequency per shift in the jet from Fig. 7.

restrict our focus to those cases in which the jet shift exceeds  $1^\circ$ , as the changes in RWB frequency for the cases with weak jet shifts do not stand out above the noise. Garfinkel et al. (2013) showed that, when jet latitude exceeds  $50^\circ$  or is less than  $35^\circ$ , the jet shift in response to a vortex is weak [consistent with Kidston and Gerber (2010), Barnes and Hartmann (2010), Son et al. (2010)], and so these cases are excluded from the analysis. Figures 8f,g show the change in RWB frequency with latitude upon imposing a vortex. RWB anomalies in the presence of a vortex are qualitatively similar to those during poleward-shifted jet events associated with internal variability: a strong vortex leads to

slightly more AWB equatorward of the jet and less CWB poleward of the jet [consistent with Wittman et al. (2007) and Ndarana et al. (2012)], though extremes in anomalous RWB frequency exist far from the jet core. The jet shift is stronger for jets near  $40^\circ$ , which is consistent with the stronger changes in RWB frequency for jets near  $40^\circ$  in Figs. 8f,g. To demonstrate the quantitative resemblance between the changes in RWB frequency per degree jet shift, cyan asterisks are included in Fig. 9 that show the changes in RWB frequency per degree jet shift for the vortex experiments in which jet shift exceeds  $4^\circ$  (i.e., the cases with the largest signal-to-noise ratio). Regardless of whether a jet shift is caused by a polar vortex or is due to

internal variability, the change in RWB frequency per degree jet shift is indistinguishable.

Finally, we consider whether there is a relationship among the changes in RWB frequency in response to a vortex, in response to the tropospheric midlatitude baroclinic forcing as described in section 3 and associated with internal variability. The change in RWB frequency per degree jet shift in response to the baroclinic forcing is represented by an error bar on the left of each panel in Fig. 9. This error bar represents the slope of the best-fit line included in each panel of Fig. 7. It is clear that the change in RWB frequency per degree jet shift is indistinguishable, regardless of the source of the jet shift.

### *c. On the inseparability of RWB and the eddy-driven jet*

We have just shown that changes in RWB are inseparable from the change in latitude of the eddy-driven jet for three different sources of jet movement. From this result, one might deduce that the eddy forcing of the jet is dominated by RWB events, and we now confirm this deduction. We demonstrate this by compositing the high-frequency EMFC in response to unforced and forced variability in days/regions where RWB occurs and also in days/regions in which RWB does not occur. As discussed in section 3, days/regions in which RWB occurs dominate the climatological EMFC near the jet core (Fig. 5a). Figure 5b shows the change in high-frequency EMFC normalized by the jet shift due to internal variability of the jet. The high-frequency EMFC is again dominated by RWB dates/regions. (Note that RWB dates/regions dominate the change in EMFC associated with internal variability in other experiments as well, which is not shown.) Finally, Fig. 5c shows the change in high-frequency EMFC normalized by the jet shift due to the inclusion of a stratospheric polar vortex. The high-frequency EMFC is again dominated by RWB dates/regions. Importantly, the changes in high-frequency EMFC associated with internal variability and with a polar vortex anomaly are quantitatively similar in RWB regions/dates and even to a lesser degree in no-RWB regions/dates. While some EMFC is not associated with RWB events but rather with wave dissipation or other processes, RWB and the eddy-driven jet are so coupled that it likely does not make sense to separate them. The crucial role of RWB for tropospheric jet shifts has also been highlighted recently by Chen et al. (2013) and Lu et al. (2014).

It is conceivable that the change in RWB frequency would be smaller if the jet latitude is set by an altered equator-to-pole temperature gradient. In this case, the jet latitude is set explicitly by the baroclinic forcing and eddies might be thought of reacting passively to this baroclinic forcing; hence, RWB frequency could

hypothetically change by less per degree of jet latitude for a baroclinic forcing. However, these experiments clearly demonstrate that such thinking is incorrect.

Finally, no evidence is found in these experiments for the mechanisms proposed by, for example, Wittman et al. (2007), Kunz et al. (2009), and Rivière (2011) in which RWB mediates the jet shift in response to an external forcing; RWB anomalies in response to an external forcing are indistinguishable from those due to internal variability. While this does not necessarily disprove these mechanisms, it does suggest that it will be very difficult to provide evidence for these mechanisms in a data source in which stochastic variability of jet latitude is present. Stated another way, these results suggest that the change in RWB per degree latitude does not depend on the time scale of the jet shift: both internal variability (in which the characteristic time scale for the jet shift is several weeks) and externally forced, long-time-scale variability lead to identical RWB anomalies.

It is interesting to note that that the magnitude of the change in RWB frequency per degree jet shift is larger for jets that are farther equatorward. In other words, a larger change in RWB frequency accompanies a jet shift for a jet near  $30^\circ$  as compared to a jet near  $50^\circ$ . These changes are also present when we focus on the strongest RWB events only (not shown). This effect is consistent with the slight deviation from linearity and kink near  $50^\circ$  shown in Fig. 7: while the best-fit line captures the distribution of RWB frequency quite well in Fig. 7, a second-order polynomial fit (not shown) suggests that a larger change in RWB frequency is associated with a given shift in jet latitude for jets near  $30^\circ$  as compared to jets near  $50^\circ$ . A thorough understanding of this effect is left for future work, though it may be related to spherical effects: a smaller change in RWB frequency is sufficient to drive a jet poleward if the jet is located closer to the pole such that a weaker torque can produce the same zonal-mean momentum forcing.

## 5. Conclusions

Rosby wave breaking (RWB) leads to impactful weather events (e.g., cutoff lows and blocking highs) and stratosphere–troposphere exchange of trace gases (Pelly and Hoskins 2003; Sprenger et al. 2007; Ndarana and Waugh 2010). Hence, it is crucial 1) to understand the climatological distribution of RWB, 2) to evaluate how the distribution of RWB events changes due to unforced and forced variability, and 3) to assess quantitatively whether changes in RWB distribution as a jet changes its meridional position depend on the cause of the shift in the jet's position.

These three aims are investigated in long integrations of a dry general circulation model. An ensemble of

experiments is performed in which jet latitude is set by varying the location of the midlatitude tropospheric baroclinicity while keeping the total equator-to-pole temperature difference constant. Specifically, eddy-driven jets are created from  $27^\circ$  to near  $54^\circ$ , which spans the latitudinal range of eddy-driven jets in Earth's atmosphere. The net effect of the baroclinic forcing resembles, in a limited but important manner, the observed tropospheric temperature trends over the satellite era. For each configuration of the equator-to-pole temperature gradient, two experiments are performed: one with a stratospheric polar vortex and one without. The distribution of RWB is computed for each experiment. Finally, for each experiment, the distribution of RWB is produced during days in which the midlatitude eddy-driven jet is equatorward shifted as compared to days in which it is poleward shifted.

The following conclusions can be drawn from these experiments:

- (i) Maxima in RWB frequency are present on either flank of the eddy-driven jet. If the eddy-driven jet is well separated from the subtropics, then a third maximum in RWB frequency is also present near the subtropical zero wind line. Very large-amplitude RWB events tend not to occur near the subtropical zero line, and they typically feed momentum into the eddy-driven jet exclusively. Nearly all of the high-frequency eddy momentum flux convergence into the jet is associated with RWB events.
- (ii) CWB frequency on the poleward flank of the jet decreases, and AWB frequency on the equatorward flank of the jet increases, as the jet latitude moves poleward. Overall, RWB frequency increases as the jet moves poleward. For cases in which the jet is poleward of  $50^\circ$ , there is, if anything, more AWB than CWB on the poleward flank of the jet.
- (iii) Internal variability of the jet is associated with a banded structure of anomalies in RWB frequency. In particular, if we composite days in which the jet is poleward shifted and days in which the jet is equatorward shifted and compare the composites, we find four or five distinct RWB anomalies. In other words, the RWB anomalies cannot be accurately summarized as more AWB equatorward of the jet and less CWB poleward of the jet. If we average near the jet core or focus on the strongest RWB events, however, we recover the conventional wisdom: a poleward shift is associated with more AWB equatorward of the jet and less CWB poleward of the jet.
- (iv) Finally but more importantly, quantitatively similar changes are present among the changes in RWB frequency in response to a stratospheric polar vortex,

to altered baroclinic forcing in the troposphere, and to internal variability of the jet. This result suggests that mechanisms involving RWB are likely not the ultimate cause for the shift in jet latitude due to a vortex or due to internal variability of the jet, as these changes in RWB occur even if the jet position is set explicitly by a thermal forcing. RWB and the eddy-driven jet are so closely coupled (and in some sense different diagnostics of same thing) that it may not make sense to try to separate cause and effect.

*Acknowledgments.* This work was supported by the NSF Grants ATM 0905863 and AGS 0938325 and by a startup grant from Hebrew University of Jerusalem. We acknowledge NCAR's Computational and Information Systems Laboratory for providing computing resources. We are very grateful to E.A. Barnes and J. Lu for helpful comments on an earlier version of this manuscript, the two anonymous reviewers for their helpful comments, T. Ndarana for useful discussions and for providing his Rossby wave-breaking code, and E. Gerber for help in conducting these experiments.

## APPENDIX

### RWB in the Dry Model and in MERRA

This appendix demonstrates that the RWB distribution with latitude in the dry model resembles closely that in MERRA and therefore that the dry model is a useful tool for analyzing how the distribution of RWB changes with jet latitude. [Figure A1](#) compares the climatological distribution of RWB in the dry model experiment in which the climatological jet latitude closely resembles that in MERRA. In both data sources, RWB frequency is lower at the jet core than at either flank of the jet, and the RWB maxima on the equatorward flank of the jet is stronger than that on the poleward flank of the jet. In addition, a secondary maximum appears on the equatorward flank of the jet in the subtropics near  $20^\circ$ . AWB dominates the RWB on the equatorward flank of the jet, while CWB dominates the RWB on the poleward flank of the jet ([Figs. A1a,d](#)). A stronger vortex and ozone depletion are associated with more RWB on the equatorward flank of the jet and fewer RWB on the poleward flank of the jet ([Figs. A1b,e](#); as in [Ndarana et al. 2012](#)). Similarly, a poleward shift of the jet associated with internal variability is associated with more frequent RWB on the equatorward flank of the jet and less frequent RWB on the poleward flank of the jet and vice versa for an equatorward shift of the jet ([Figs. A1c,f](#)).

Note that the dry model simulates more RWB events than MERRA (cf. the values on the ordinate in [Fig. A1](#)).

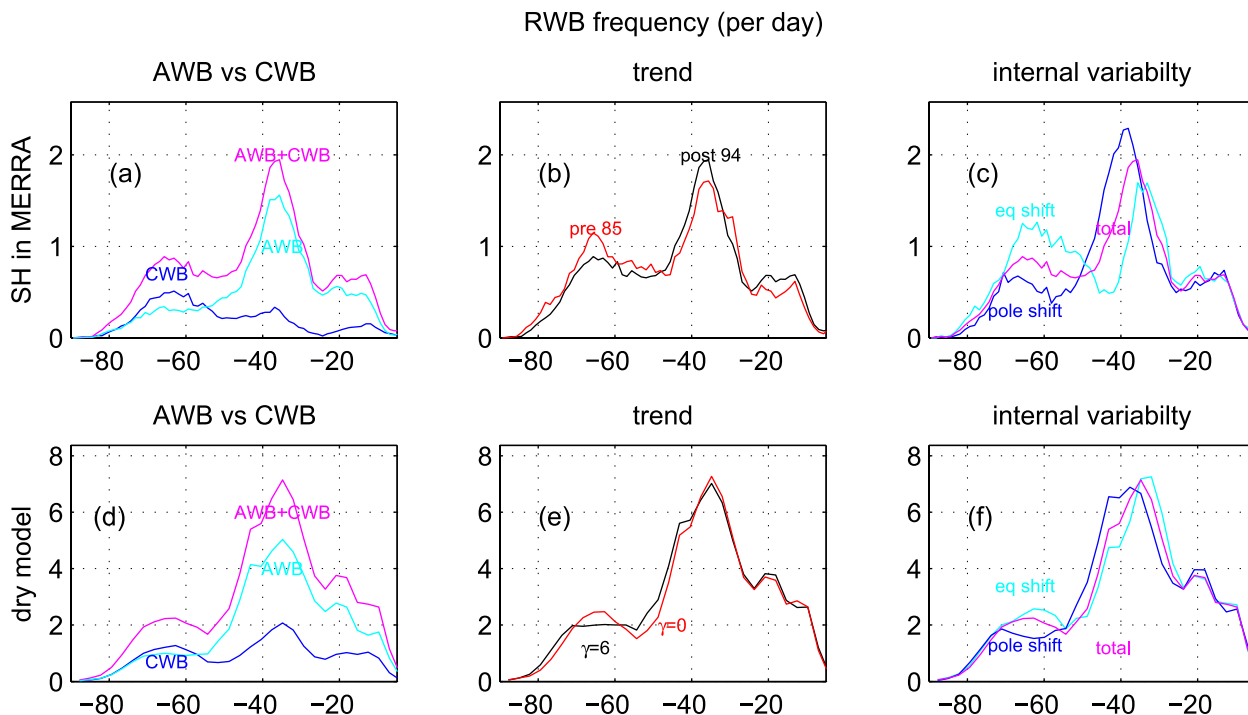


FIG. A1. RWB in the SH in December–February (DJF) in MERRA as compared to a dry model case in which the jet latitude most closely resembles that in MERRA: (a) climatological breakdown between AWB and CWB; (b) distribution during the pre-ozone-hole era and the ozone-hole era; and (c) response to internal variability. (d)–(f) As in (a)–(c), but for the dry model; for (e), we compare the integration with  $\gamma = 6$  to the integrations with  $\gamma = 0$ . As discussed in the text, there are more RWB in the dry model than in MERRA.

This result is robust to removing duplicate events or specific contours on which RWB is detected or to focusing on the hemisphere without topography. Future work is needed to fully understand why this difference might exist. However, a sensitivity experiment has been performed in which the total equator-to-pole temperature difference is set to 40 K instead of 60 K, and in this experiment the RWB frequency matches more closely the RWB frequency in MERRA. Lowering the equator-to-pole temperature difference does not affect the distribution of RWB with latitude, which implies that the distribution with latitude of RWB (i.e., the focus of this paper) is independent of its total frequency.

#### REFERENCES

- Akahori, K., and S. Yoden, 1997: Zonal flow vacillation and bimodality of baroclinic eddy life cycles in a simple global circulation model. *J. Atmos. Sci.*, **54**, 2349–2361, doi:10.1175/1520-0469(1997)054<2349:ZFVABO>2.0.CO;2.
- Allen, R. J., S. C. Sherwood, J. R. Norris, and C. S. Zender, 2012: Recent Northern Hemisphere tropical expansion primarily driven by black carbon and tropospheric ozone. *Nature*, **485**, 350–354, doi:10.1038/nature11097.
- Barnes, E. A., and D. L. Hartmann, 2010: Testing a theory for the effect of latitude on the persistence of eddy-driven jets using CMIP3 simulations. *Geophys. Res. Lett.*, **37**, L15801, doi:10.1029/2010GL044144.
- , and —, 2012: Detection of Rossby wave breaking and its response to shifts of the midlatitude jet with climate change. *J. Geophys. Res.*, **117**, D09117, doi:10.1029/2012JD017469.
- , and L. Polvani, 2013: Response of the midlatitude jets, and of their variability, to increased greenhouse gases in the CMIP5 models. *J. Climate*, **26**, 7117–7135, doi:10.1175/JCLI-D-12-00536.1.
- Benedict, J. J., S. Lee, and S. B. Feldstein, 2004: Synoptic view of the North Atlantic Oscillation. *J. Atmos. Sci.*, **61**, 121–144, doi:10.1175/1520-0469(2004)061<0121:SVOTNA>2.0.CO;2.
- Branstator, G., 1995: Organization of storm track anomalies by recurring low-frequency circulation anomalies. *J. Atmos. Sci.*, **52**, 207–226, doi:10.1175/1520-0469(1995)052<0207:OOSTAB>2.0.CO;2.
- Ceppi, P., M. D. Zelinka, and D. L. Hartmann, 2014: The response of the southern hemispheric eddy-driven jet to future changes in shortwave radiation in CMIP5. *Geophys. Res. Lett.*, **41**, 3244–3250, doi:10.1002/2014GL060043.
- Chen, G., J. Lu, and L. Sun, 2013: Delineating the eddy–zonal flow interaction in the atmospheric circulation response to climate forcing: Uniform SST warming in an idealized aquaplanet model. *J. Atmos. Sci.*, **70**, 2214–2233, doi:10.1175/JAS-D-12-0248.1.
- Edmon, H. J., Jr., B. J. Hoskins, and M. E. McIntyre, 1980: Eliassen–Palm cross sections for the troposphere. *J. Atmos.*

- Sci.*, **37**, 2600–2616, doi:10.1175/1520-0469(1980)037<2600:EPCSFT>2.0.CO;2.
- Esler, J., and P. Haynes, 1999: Baroclinic wave breaking and the internal variability of the tropospheric circulation. *J. Atmos. Sci.*, **56**, 4014–4031, doi:10.1175/1520-0469(1999)056<4014:BWBATI>2.0.CO;2.
- Feldstein, S., and S. Lee, 1998: Is the atmospheric zonal index driven by an eddy feedback? *J. Atmos. Sci.*, **55**, 3077–3086, doi:10.1175/1520-0469(1998)055<3077:ITAZID>2.0.CO;2.
- Franzke, C., S. Lee, and S. B. Feldstein, 2004: Is the North Atlantic Oscillation a breaking wave? *J. Atmos. Sci.*, **61**, 145–160, doi:10.1175/1520-0469(2004)061<0145:ITNAOA>2.0.CO;2.
- , S. B. Feldstein, and S. Lee, 2011: Synoptic analysis of the Pacific–North American teleconnection pattern. *Quart. J. Roy. Meteor. Soc.*, **137**, 329–346, doi:10.1002/qj.768.
- Fu, Q., C. M. Johanson, J. M. Wallace, and T. Reichler, 2006: Enhanced mid-latitude tropospheric warming in satellite measurements. *Science*, **312**, 1179, doi:10.1126/science.1125566.
- Garfinkel, C. L., D. W. Waugh, and E. P. Gerber, 2013: The effect of tropospheric jet latitude on coupling between the stratospheric polar vortex and the troposphere. *J. Climate*, **26**, 2077–2095, doi:10.1175/JCLI-D-12-00301.1.
- Gerber, E. P., and L. M. Polvani, 2009: Stratosphere–troposphere coupling in a relatively simple AGCM: The importance of stratospheric variability. *J. Climate*, **22**, 1920–1933, doi:10.1175/2008JCLI2548.1.
- Gong, T., S. B. Feldstein, and D. Luo, 2010: The impact of ENSO on wave breaking and southern annular mode events. *J. Atmos. Sci.*, **67**, 2854–2870, doi:10.1175/2010JAS3311.1.
- Hartmann, D. L., 1995: A PV view of zonal flow vacillation. *J. Atmos. Sci.*, **52**, 2561–2576, doi:10.1175/1520-0469(1995)052<2561:APVOZF>2.0.CO;2.
- Held, I. M., 1975: Momentum transport by quasi-geostrophic eddies. *J. Atmos. Sci.*, **32**, 1494–1496, doi:10.1175/1520-0469(1975)032<1494:MTBQGE>2.0.CO;2.
- , and M. J. Suarez, 1994: A proposal for the intercomparison of the dynamical cores of atmospheric general circulation models. *Bull. Amer. Meteor. Soc.*, **75**, 1825–1830, doi:10.1175/1520-0477(1994)075<1825:APFTIO>2.0.CO;2.
- Hoskins, B. J., I. N. James, and G. H. White, 1983: The shape, propagation and mean-flow interaction of large-scale weather systems. *J. Atmos. Sci.*, **40**, 1595–1612, doi:10.1175/1520-0469(1983)040<1595:TSPAMF>2.0.CO;2.
- Kidston, J., and E. P. Gerber, 2010: Intermodel variability of the poleward shift of the austral jet stream in the CMIP3 integrations linked to biases in 20th century climatology. *Geophys. Res. Lett.*, **37**, L09708, doi:10.1029/2010GL042873.
- Kunz, T., K. Fraedrich, and F. Lunkeit, 2009: Response of idealized baroclinic wave life cycles to stratospheric flow conditions. *J. Atmos. Sci.*, **66**, 2288–2302, doi:10.1175/2009JAS2827.1.
- Lorenz, D. J., 2014: Understanding midlatitude jet variability and change using Rossby wave chromatography: Poleward shifted jets in response to external forcing. *J. Atmos. Sci.*, **71**, 2370–2389, doi:10.1175/JAS-D-13-0200.1.
- , and D. L. Hartmann, 2001: Eddy-zonal flow feedback in the Southern Hemisphere. *J. Atmos. Sci.*, **58**, 3312–3326, doi:10.1175/1520-0469(2001)058<3312:EZFFIT>2.0.CO;2.
- Lu, J., L. Sun, Y. Wu, and G. Chen, 2014: The role of subtropical irreversible PV mixing in the zonal mean circulation response to global warming-like thermal forcing. *J. Climate*, **27**, 2297–2316, doi:10.1175/JCLI-D-13-00372.1.
- Martius, O., C. Schwierz, and H. Davies, 2007: Breaking waves at the tropopause in the wintertime Northern Hemisphere: Climatological analyses of the orientation and the theoretical LC1/2 classification. *J. Atmos. Sci.*, **64**, 2576–2592, doi:10.1175/JAS3977.1.
- Ndarana, T., and D. W. Waugh, 2010: The link between cut-off lows and Rossby wave breaking in the Southern Hemisphere. *Quart. J. Roy. Meteor. Soc.*, **136**, 869–885, doi:10.1002/qj.627.
- , and —, 2011: A climatology of Rossby wave breaking on the Southern Hemisphere tropopause. *J. Atmos. Sci.*, **68**, 798–811, doi:10.1175/2010JAS3460.1.
- , —, L. M. Polvani, G. J. P. Correa, and E. P. Gerber, 2012: Antarctic ozone depletion and trends in tropopause Rossby wave breaking. *Atmos. Sci. Lett.*, **13**, 164–168, doi:10.1002/asl.384.
- Pelly, J. L., and B. J. Hoskins, 2003: A new perspective on blocking. *J. Atmos. Sci.*, **60**, 743–755, doi:10.1175/1520-0469(2003)060<0743:ANPOB>2.0.CO;2.
- Polvani, L. M., and P. J. Kushner, 2002: Tropospheric response to stratospheric perturbations in a relatively simple general circulation model. *Geophys. Res. Lett.*, **29**, doi:10.1029/2001GL014284.
- Rienecker, M. M., and Coauthors, 2011: MERRA: NASA's Modern-Era Retrospective Analysis for Research and Applications. *J. Climate*, **24**, 3624–3648, doi:10.1175/JCLI-D-11-00015.1.
- Rivière, G., 2009: Effect of latitudinal variations in low-level baroclinicity on eddy life cycles and upper-tropospheric wave-breaking processes. *J. Atmos. Sci.*, **66**, 1569–1592, doi:10.1175/2008JAS2919.1.
- , 2011: A dynamical interpretation of the poleward shift of the jet streams in global warming scenarios. *J. Atmos. Sci.*, **68**, 1253–1272, doi:10.1175/2011JAS3641.1.
- , and I. Orlanski, 2007: Characteristics of the Atlantic storm-track eddy activity and its relation with the North Atlantic Oscillation. *J. Atmos. Sci.*, **64**, 241–266, doi:10.1175/JAS3850.1.
- Robinson, W. A., 1996: Does eddy feedback sustain variability in the zonal index? *J. Atmos. Sci.*, **53**, 3556–3569, doi:10.1175/1520-0469(1996)053<3556:DEFSVI>2.0.CO;2.
- Simmons, A. J., and B. J. Hoskins, 1978: The life cycles of some nonlinear baroclinic waves. *J. Atmos. Sci.*, **35**, 414–432, doi:10.1175/1520-0469(1978)035<0414:TLCOSN>2.0.CO;2.
- Son, S.-W., and Coauthors, 2010: Impact of stratospheric ozone on Southern Hemisphere circulation change: A multimodel assessment. *J. Geophys. Res.*, **115**, D00M07, doi:10.1029/2010JD014271.
- Sprenger, M., H. Wernli, and M. Bourqui, 2007: Stratosphere–troposphere exchange and its relation to potential vorticity streamers and cutoffs near the extratropical tropopause. *J. Atmos. Sci.*, **64**, 1587–1602, doi:10.1175/JAS3911.1.
- Strong, C., and G. Magnusdottir, 2008: Tropospheric Rossby wave breaking and the NAO/NAM. *J. Atmos. Sci.*, **65**, 2861–2876, doi:10.1175/2008JAS2632.1.
- Tandon, N. F., E. P. Gerber, A. H. Sobel, and L. M. Polvani, 2013: Understanding Hadley cell expansion versus contraction: Insights from simplified models and implications for recent observations. *J. Climate*, **26**, 4304–4321, doi:10.1175/JCLI-D-12-00598.1.
- Thorncroft, C. D., B. J. Hoskins, and M. E. McIntyre, 1993: Two paradigms of baroclinic-wave life-cycle behaviour. *Quart. J. Roy. Meteor. Soc.*, **119**, 17–55, doi:10.1002/qj.49711950903.

- Wang, Y.-H., and G. Magnustdottir, 2011: Tropospheric Rossby wave breaking and the SAM. *J. Climate*, **24**, 2134–2146, doi:[10.1175/2010JCLI4009.1](https://doi.org/10.1175/2010JCLI4009.1).
- Wilcox, L. J., A. Charlton-Perez, and L. J. Gray, 2012: Trends in austral jet position in ensembles of high-and low-top CMIP5 models. *J. Geophys. Res.*, **117**, D13115, doi:[10.1029/2012JD017597](https://doi.org/10.1029/2012JD017597).
- Wittman, M. A. H., L. M. Polvani, R. K. Scott, and A. J. Charlton, 2004: Stratospheric influence on baroclinic lifecycles and its connection to the Arctic Oscillation. *Geophys. Res. Lett.*, **31**, L16113, doi:[10.1029/2004GL020503](https://doi.org/10.1029/2004GL020503).
- , A. J. Charlton, and L. M. Polvani, 2007: The effect of lower stratospheric shear on baroclinic instability. *J. Atmos. Sci.*, **64**, 479–496, doi:[10.1175/JAS3828.1](https://doi.org/10.1175/JAS3828.1).
- Woollings, T., B. Hoskins, M. Blackburn, and P. Berrisford, 2008: A new Rossby wave–breaking interpretation of the North Atlantic Oscillation. *J. Atmos. Sci.*, **65**, 609–626, doi:[10.1175/2007JAS2347.1](https://doi.org/10.1175/2007JAS2347.1).
- Yu, J., and D. L. Hartmann, 1993: Zonal flow vacillation and eddy forcing in a simple GCM of the atmosphere. *J. Atmos. Sci.*, **50**, 3244–3259, doi:[10.1175/1520-0469\(1993\)050<3244:ZFVAEF>2.0.CO;2](https://doi.org/10.1175/1520-0469(1993)050<3244:ZFVAEF>2.0.CO;2).